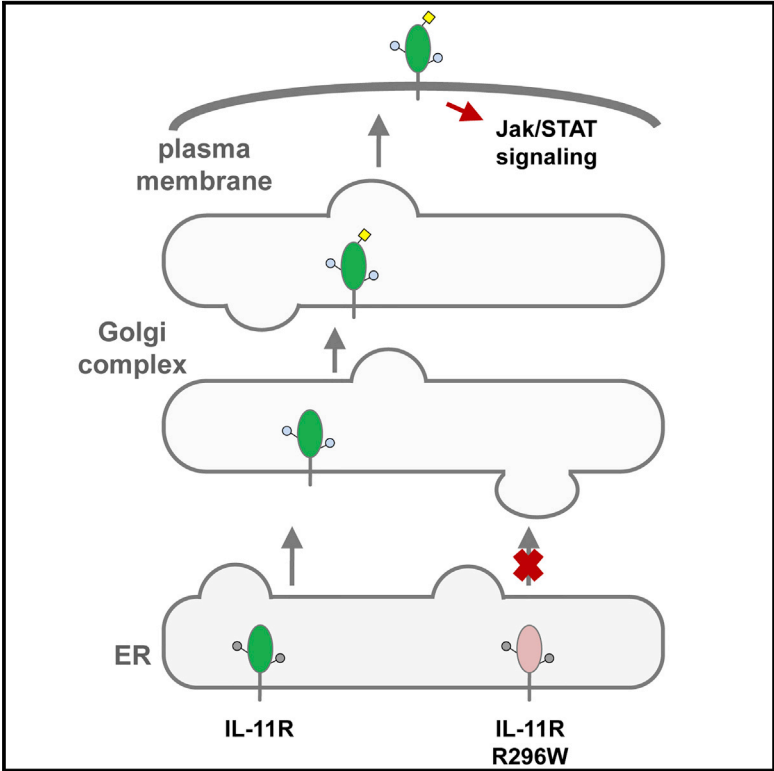# Cell Reports

Mutations in Craniosynostosis Patients Cause Defective Interleukin-11 Receptor Maturation and Drive Craniosynostosis-like Disease in Mice

Graphical Abstract

Authors

Maria Agthe, Julian Brügge, Yvonne Garbers, ..., Tracy Putoczki, Joachim Grötzinger, Christoph Garbers

Correspondence

christoph.garbers@med.ovgu.de

In Brief

Mutations within the IL-11R cause craniosynostosis, a malformation of the skull. Agthe et al. show that some of these mutations prevent maturation of the IL-11R and identify structural traits whose disturbance causes misfolding of the receptor. They find that signaling via the membrane-bound IL-11R is required for skull formation.

Highlights

- Mutations within the IL-11R cause craniosynostosis in human patients

- Mutations prevent IL-11R maturation and cause intracellular retention

- Disruption of a conserved arginine-tryptophan zipper causes IL-11R misfolding

- IL-11 classic signaling is required for proper skull formation in mice

CellPress

Mutations in Craniosynostosis Patients Cause Defective Interleukin-11 Receptor Maturation and Drive Craniosynostosis-like Disease in Mice

Maria Agthe,[1] Julian Brügge,[1] Yvonne Garbers,[2] Marieke Wandel,[1] Birte Kespohl,[1] Philipp Arnold,[3] Charlotte M. Flynn,[1] Juliane Lokau,[1,7] Samadhi Aparicio-Siegmund,[1] Christian Bretscher,[1] Stefan Rose-John,[1] Georg H. Waetzig,[4] Tracy Putoczki,[5,6] Joachim Grötzinger,[1] and Christoph Garbers[1,7,8,*]
[1]Institute of Biochemistry, Kiel University, Kiel, Germany
[2]Institute of Psychology, Kiel University, Kiel, Germany
[3]Institute of Anatomy, Kiel University, Kiel, Germany
[4]CONARIS Research Institute AG, Kiel, Germany
[5]The Walter and Eliza Hall Institute for Medical Research, Parkville, VIC, Australia
[6]Department of Medical Biology, The University of Melbourne, Parkville, VIC, Australia
[7]Present address: Department of Pathology, Otto-von-Guericke-University Magdeburg, Medical Faculty, Magdeburg, Germany
[8]Lead Contact
*Correspondence: christoph.garbers@med.ovgu.de
https://doi.org/10.1016/j.celrep.2018.09.005

SUMMARY

Premature closure of the sutures that connect the cranial bones during development of the mammalian skull results in a phenotype called craniosynostosis. Recently, several craniosynostosis patients with missense mutations within the gene encoding the interleukin-11 receptor (IL-11R) have been described, but the underlying molecular mechanisms have remained elusive. IL-11 is a cytokine that has a crucial role in bone remodeling and activates cells via binding to the IL-11R. Here, we show that patient mutations prevented maturation of the IL-11R, resulting in endoplasmic reticulum retention and diminished cell surface appearance. Disruption of a conserved tryptophan-arginine zipper within the third domain of the IL-11R was the underlying cause of the defective maturation. IL-11 classic signaling via the membrane-bound receptor, but not IL-11 *trans*-signaling via the soluble receptor, was the crucial pathway for normal skull development in mice *in vivo*. Thus, the specific therapeutic inhibition of IL-11 *trans*-signaling does not interfere with skull development.

INTRODUCTION

The development of the mammalian skull is a complex process involving a variety of coordinated signaling processes, including signaling via the fibroblast growth factor receptors. The skull is formed from five individual bones, which are connected at their margins via so-called sutures, ensuring that the skull is able to grow as the brain increases in size during development (Morriss-Kay and Wilkie, 2005). Closure of the sutures, which terminates skull growth, is a highly regulated process that depends on the activity of the osteoblast precursors located at the sutures

(Rice, 2005). Craniosynostosis is defined as the premature closure of cranial sutures, which often happens prenatally, and is diagnosed at a rate of 1:2,500 among newborns.

Recently, several missense mutations in the gene *IL11RA* (encoding the interleukin-11 receptor) have been described in human patients (Clarke et al., 2018; Keupp et al., 2013; Nieminen et al., 2011). The affected individuals are described to display a Crouzon-like craniosynostosis phenotype, including multiple suture synostosis and delayed tooth eruption. Furthermore, some individuals have supernumerary teeth (Nieminen et al., 2011) and conductive hearing loss (Keupp et al., 2013). The mutations are distributed over the entire extracellular part of the IL-11R, but the majority are located within the D3 domain. Initial experiments suggested that the mutations inactivated the receptor and caused the observed phenotypes (Keupp et al., 2013; Nieminen et al., 2011). However, how the mutations affect the biological function of the IL-11R has not been investigated, and the underlying molecular and structural mechanisms are unknown.

Interleukin-11 (IL-11) is a member of the IL-6 family of cytokines that is poorly characterized (Garbers et al., 2012; Garbers and Scheller, 2013). It can activate the hepatic acute phase response (Baumann and Schendel, 1991) and was most recently identified as a prominent driver of gastrointestinal tumorigenesis (Putoczki et al., 2013). IL-11 activates its target cells through binding to the IL-11R, which in turn leads to the recruitment of a homodimer of the signal-transducing β-receptor gp130 and the activation of intracellular signaling cascades (Garbers et al., 2012). The expression of the IL-11R determines which cells can be activated by the cytokine, while gp130 is expressed ubiquitously. The IL-11R is expressed on a variety of different cell types and tissues, including intestine, spleen, heart, and lung (Davidson et al., 1997; Putoczki and Ernst, 2010) and acts as a transcytosis receptor for IL-11 on polarized cells (Monhasery et al., 2016). Importantly, the IL-11R is also found on osteoblasts, and signaling via the IL-11R is required for normal bone remodeling in mice. Consequently, *Il11ra*$^{-/-}$ mice have reduced length of the long bones (Sims et al.,

2005), and a SNP in IL-11, which is associated with reduced adult height in humans, reduces the biological activity of the cytokine (Lokau et al., 2018).

In addition to signaling through the membrane-bound IL-11R, which is termed classic signaling, there is recent evidence that IL-11 can also signal through soluble forms of the IL-11R (sIL-11R) (Lokau et al., 2016a, 2017). Importantly, the anti-inflammatory compound sgp130Fc, which is currently in phase 2 clinical trials, blocks this so-called IL-11 *trans*-signaling pathway but does not influence signaling of IL-11 via the membrane-bound receptor (Lokau et al., 2016b).

In the present study, we analyzed prominent IL-11R patient mutations and confirmed that they were deleterious for IL-11 signaling. We further found that the mutated receptors were not transported to the cell surface, had defective maturation, and were predominantly retained within the endoplasmic reticulum (ER). We identified the disturbance of a conserved tryptophan-arginine zipper, which is common to all cytokine receptors (Olsen and Kragelund, 2014), as the underlying cause of the misfolding of the IL-11R. Finally, we showed *in vivo* that IL-11 signaling, but not signaling of the cognate cytokine IL-6, is crucial for correct formation of the skull, and identified IL-11 classic signaling as the responsible signaling pathway in mice.

RESULTS

The Patient Mutations R296W, P200T, and P221R Impair the Biological Activity of the IL-11R

IL-11R patient mutations are distributed over the whole ectodomain (Figure 1A). We first sought to verify lack of biological activity for the mutations R296W, P200T, and P221R and generated Ba/F3-gp130 cell lines that stably express the different IL-11R variants. In contrast to Ba/F3-gp130-IL-11R cells (Figure 1B), Ba/F3-gp130 cells stably expressing IL-11R-R296W, IL-11R-P200T, or IL-11R-P221R did not proliferate in response to IL-11 (Figures 1C–1E). Furthermore, IL-11 treatment resulted in phosphorylation of STAT3 only in Ba/F3-gp130-IL-11R cells (Figure 1F). In summary, our data confirm that R296W, P200T, and P221R are mutations that abrogate the biological activity of the IL-11R.

IL-11R Variants Containing R296W, P200T, or P221R Do Not Mature Properly, and IL-11R-R296W Is Predominantly Localized in the ER

Western blot analysis of lysates of the Ba/F3-gp130-IL-11R cells revealed at least three distinct bands, while the three cell lines expressing the mutants lacked the band with the highest apparent molecular weight (Figure 1F), suggesting impaired maturation (glycosylation) of these receptors along the secretory pathway. We confirmed this in HEK293 cells (Figure S1A) and additionally observed no sIL-11R generation in cells expressing the patient mutations (Figure S1A). Flow cytometry analyses indicated that the impaired maturation prevented transport of the IL-11R variants to the cell surface (Figures S1B–S1D).

The IL-11R is a glycoprotein that has two N-linked glycans and an unknown number of O-glycans (Agthe et al., 2018).

Because N-linked glycans are initially attached in the ER and finally modified in the Golgi apparatus, whereas O-linked glycans are attached later within the Golgi apparatus, the glycosylation status of a glycoprotein can be used to monitor maturation and transport through the secretory pathway. Therefore, we expressed IL-11R-WT (wild-type) and IL-11R-R296W transiently in HEK293 cells and incubated the lysate with PNGaseF or EndoH or left them untreated. EndoH is able to remove only the so-called high mannose form of N-glycans, which are attached in the ER, whereas PNGaseF can cleave all variants of N-linked glycans. As shown in Figure 2A, parts of the IL-11R-WT were resistant to cleavage by EndoH but were susceptible to PNGaseF treatment. In contrast, the IL-11R-R296W variant was equally and fully susceptible to both EndoH and PNGaseF. To further strengthen this point, we added the ER retention motif KKSS to the C terminus of the IL-11R in order to create an IL-11R that was inherently retained within the ER. The resulting IL-11R-KKSS variant behaved like IL-11R-R296W (Figures 2B–2D). Furthermore, we found strong co-staining of the *cis*-Golgi matrix protein GM130 and IL-11R-WT, which was significantly lower for both IL-11R-R296W and IL-11R-KKSS (Figures 2E and 2F). Collectively, these data show that the observed defect in maturation is caused by retention within the ER.

The IL-11R Tolerates Different Amino Acid Residues at Position 296

The patient mutation R296W results in the exchange of an amino acid residue with a large basic aliphatic chain (arginine) to a residue with a large, bulky, and hydrophobic heterocycle (tryptophan). Therefore, we sought to analyze whether the loss of the arginine or the gain of the tryptophan causes the defect in the IL-11R. For this purpose, we introduced all 20 proteinogenic amino acids at position 296 of the IL-11R and analyzed their cell surface expression using flow cytometry. As shown in Figure 3A, the basic amino acids lysine (K; 90.7% ± 21.1% of IL-11R-WT) and histidine (H; 79.6% ± 12.4%) were tolerated at this position and resulted in comparable cell surface expression as the WT IL-11R. The same was true for the hydrophobic amino acids alanine (A; 92.1% ± 19.5%) and valine (V; 81.1% ± 20.1%), whereas the introduction of all other amino acids resulted in reduced cell surface levels of the IL-11R. Of note, R296W had the lowest cell surface appearance of all 20 IL-11R variants (27.2% ± 11.3%). The band pattern observed in HEK293 cell lysates for IL-11R-R296A and IL-11R-R296K did not differ from IL-11R-WT (Figure 3B). Both variants were also present at the cell surface of Ba/F3-gp130 cell lines and were biologically active (Figures 3C and 3D).

In order to analyze *trans*-signaling, we introduced a stop codon within the stalk region of IL-11R-WT, IL-11R-R296W, IL-11R-R296A, and IL-11R-R296K (designated sIL-11R-WT, sIL-11R-R296W, sIL-11R-R294A, and sIL-11R-R296K) and transiently transfected HEK293 cells with the resulting constructs. Like its full-length counterpart, sIL-11R-R296W was expressed but not secreted, while the three other sIL-11R variants were efficiently released into the supernatant (Figure 3E). We incubated Ba/F3-gp130 cells with these supernatants and found that all
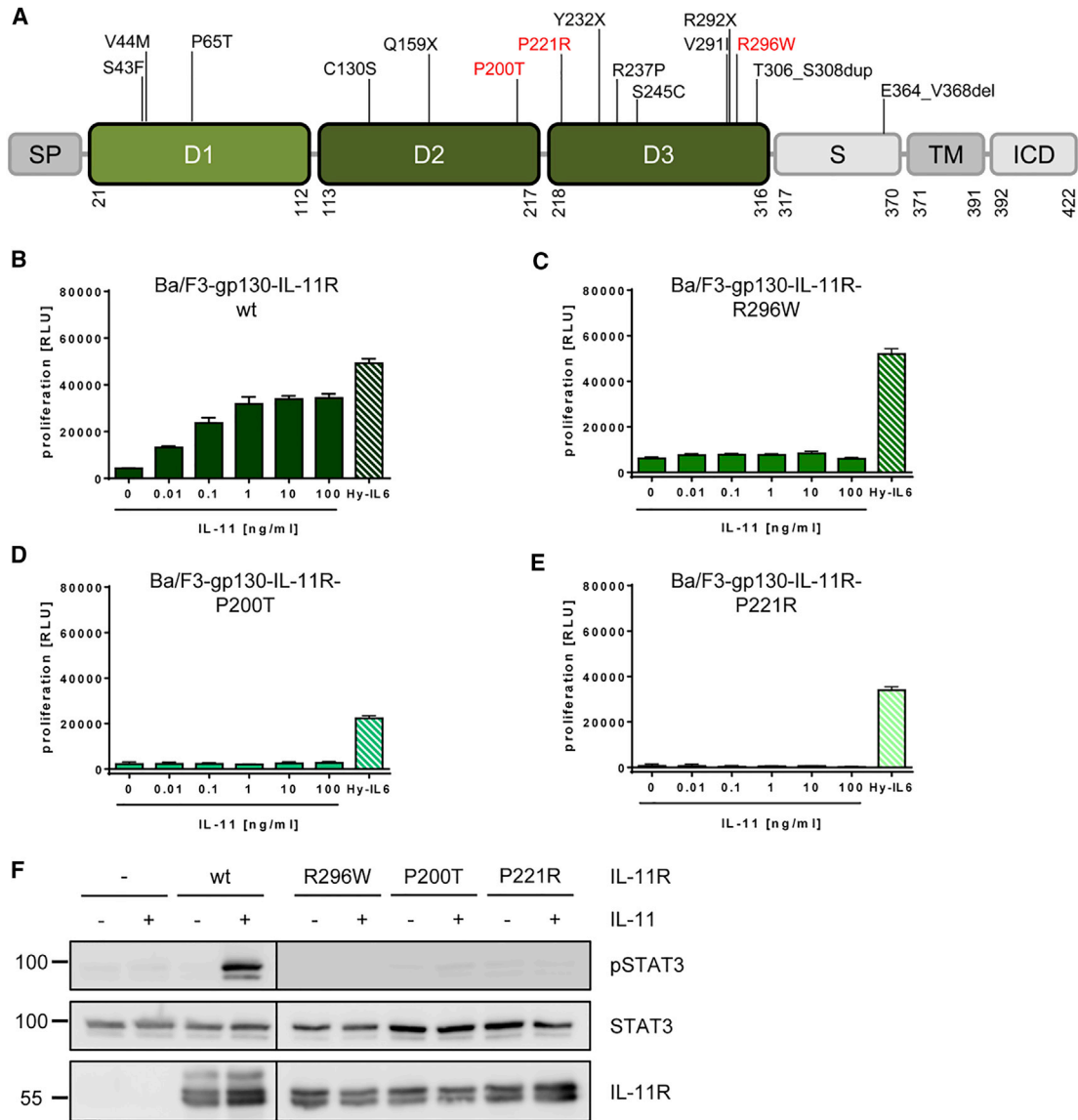
Figure 1. IL-11R Mutations from Human Craniosynostosis Patients Lead to Abrogated IL-11 Signaling

(A) Distribution of mutations described in the *IL11RA* gene that are causative for an observed craniosynostosis phenotype. Mutations highlighted in red are further analyzed in this study. Amino acids are indicated in one letter code. D1–D3, domains 1–3; del, deletion; dup, duplication; ICD, intracellular domain; S, stalk region; SP, signal peptide; TM, transmembrane region; X, premature stop codon.

(B–E) Equal numbers of Ba/F3-gp130 cells stably transduced with the indicated IL-11R variants were stimulated with increasing concentrations of recombinant IL-11, left untreated, or stimulated with 10 ng/mL hyper-IL-6 (Hy-IL-6) as a positive control. Cell viability was measured after 48 hr. One representative experiment out of three is shown (mean ± SD). (B) Ba/F3-gp130-IL-11R-WT, (C) Ba/F3-gp130-IL-11R-R296W, (D) Ba/F3-gp130-IL-11R-P200T, and (E) Ba/F3-gp130-IL-11R-P221R. RLU, relative light units; wt, wild-type.

(F) The cell clones characterized in (B)–(E) were stimulated with 10 ng/mL IL-11 or left untreated and harvested after 15 min. Cell lysates were analyzed for STAT3 phosphorylation. One representative blot of three is shown.

See also Figure S1.

variants, except the non-secreted sIL-11R-R296W, were biologically active (Figures 3F and 3G).

Because of the intracellular retention of the IL-11R-R296W mutant, our experiments could not address directly whether this variant was biologically active if it reached the cell surface. To circumvent this limitation, we expressed sIL-11R-WT and sIL-11R-R296W in HEK293 cells, lysed the cells, and incubated the lysates with recombinant IL-11 and sgp130Fc. Sgp130Fc is able to specifically bind IL-11/sIL-11R complexes but has no affinity to the sIL-11R alone (Lokau et al., 2016b). We precipitated sgp130Fc and proteins bound to it via incubation with protein G-agarose beads, which were afterward analyzed using western blot. Indeed,
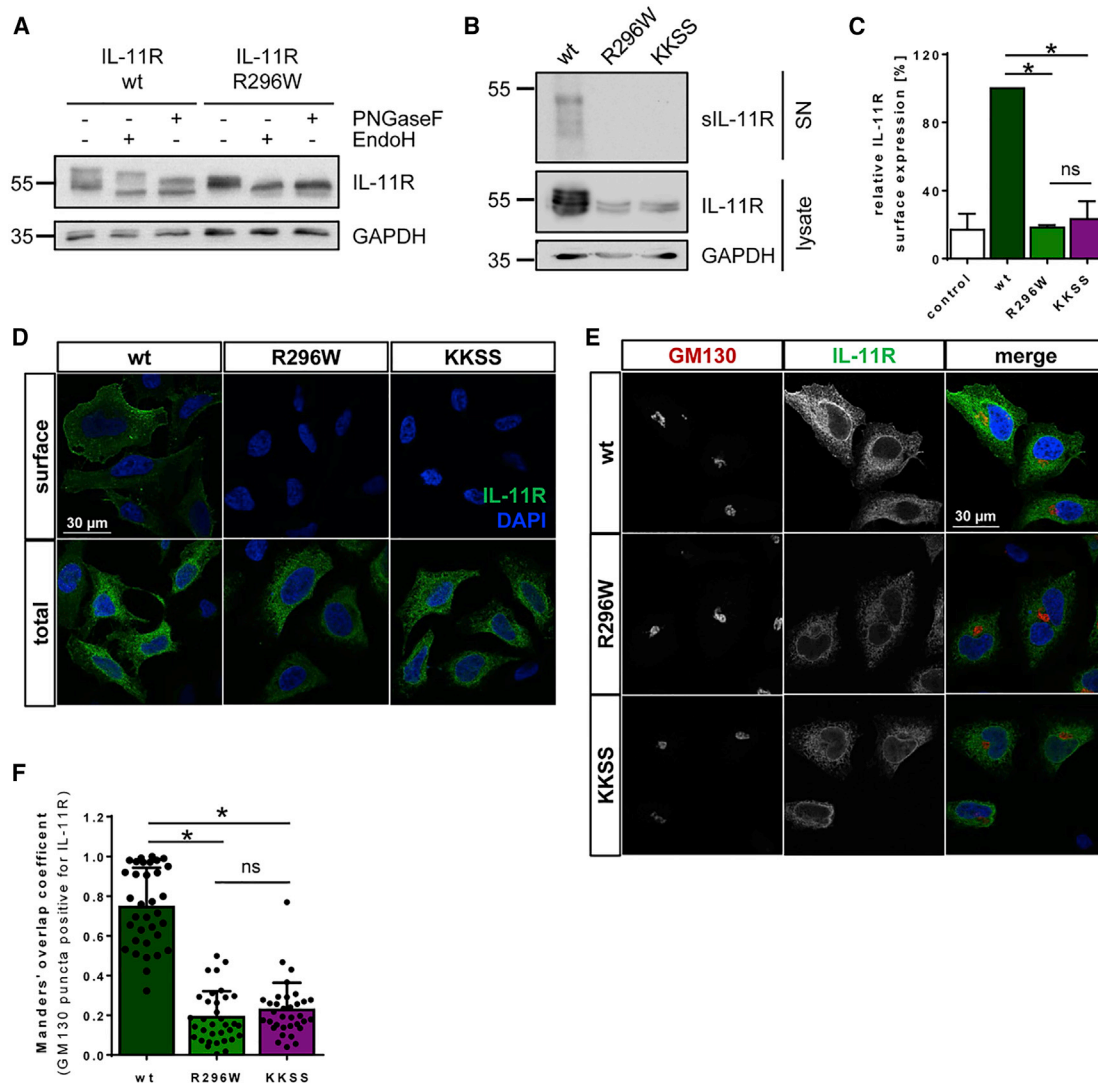
Figure 2. IL-11R-R296W Is Retained in the ER

(A) Lysates of HEK293 cells expressing IL-11R-WT or the mutant IL-11R-R296W were deglycosylated overnight using EndoH or PNGaseF and then subjected to western blot analysis. GAPDH was analyzed to ensure equal loading. The western blots shown are representative of three independent experiments.

(B) HEK293 cells were transiently transfected with IL-11R-WT, IL-11R-R296W, or an IL-11R variant fused to a C-terminal ER retention signal (IL-11R-KKSS). Constitutive receptor shedding (6 hr) was examined in TCA-precipitated cell culture supernatant (SN), and receptor expression was monitored in whole-cell lysates via western blotting. GAPDH was analyzed to ensure equal loading. Western blots shown are representative of three independent experiments.

(C) Cell surface expression of IL-11R-WT, IL-11R-R296W, and IL-11R-KKSS in transiently transfected HEK293 cells was measured via flow cytometry 48 hr after transient transfection. Untransfected cells served as negative control (control). Quantification of the mean fluorescent intensity (mean ± SD) normalized to the wild-type expression (100%) of three independent experiments is shown (ANOVA, F[3, 20] = 244.1, *p < 0.05).

(D) HeLa cells were seeded on coverslips and transiently transfected with plasmids as described in (B). Forty-eight hours after transfection, cells were fixed and stained using a blocking solution with saponin (total staining) or without saponin (surface staining). Stained slides were visualized on a confocal microscope. Scale bar, 30 μm.

(E) HeLa cells were prepared as described in (D), but all cells were permeabilized and stained for the different IL-11R variants (green) and endogenous Golgi protein GM130 (red). Slides were analyzed for IL-11R and GM130 co-localization on a confocal microscope. Scale bar, 30 μm.

(F) Manders' overlap coefficient M2 for GM130 and IL-11R. Quantification of 32 cells from three independent experiments per IL-11R variant as depicted in (E) was performed (ANOVA, F[2, 99] = 130.7, *p < 0.05). Mean ± SD is shown.

we could pull down sIL-11R-WT in complex with IL-11 by sgp130Fc (Figure 3H, lane 4) but could not detect binding of sIL-11R-R296W (Figure 4H, lane 7), although both proteins were equally well expressed in the cell lysate (Figure 3H, lanes 8 and 9).

In conclusion, we show that position 296 of the IL-11R tolerates a variety of amino acid residues and that the R296W mutation not only prevents the expression of the IL-11R at the cell surface but also renders the IL-11R biologically inactive.
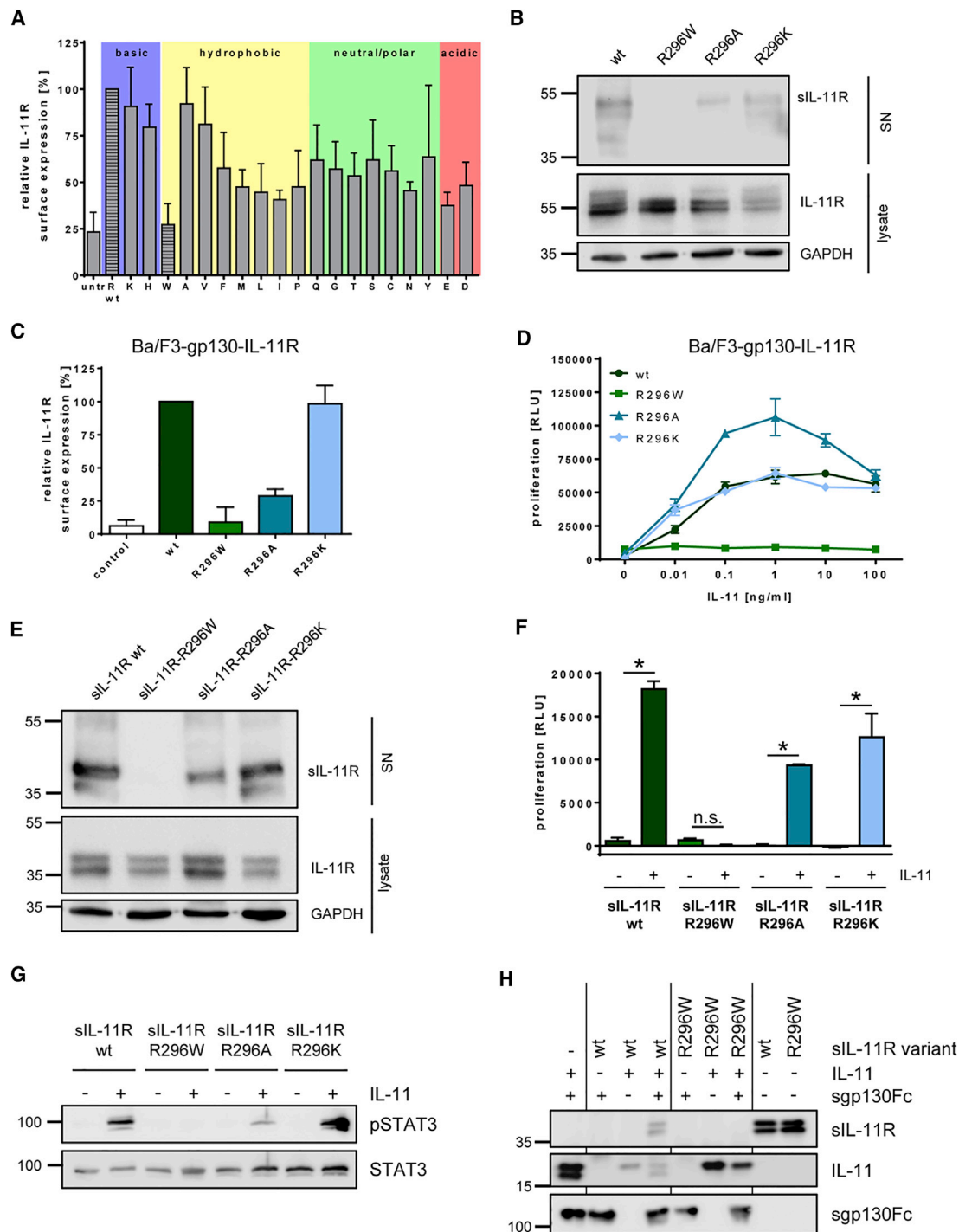
Figure 3. The IL-11R Tolerates Different Amino Acid Residues at Position 296

(A) Cell surface expression of IL-11R mutants containing all 20 proteinogenic amino acids at position 296 was measured using flow cytometry in transiently transfected HEK293 cells. Mean fluorescence intensities (mean ± SD) normalized to the wild-type expression (100%) of at least three independent experiments are depicted. Untr, untransfected; wt, wild-type.

(B) HEK293 cells were transiently transfected with the indicated IL-11R variants, and constitutive receptor shedding (6 hr) was examined in TCA-precipitated cell culture supernatants (SNs) via western blot. Cells were lysed, and IL-11R expression and maturation were analyzed using western blot. GAPDH levels served as loading control.

(C) Ba/F3-gp130 cells were stably transduced with the depicted IL-11R variants, and IL-11R cell surface expression was measured as described in (A).

(legend continued on next page)

A

B

C

D

Figure 4. The Tryptophan-Arginine Zipper in Domain D3 Is Essential for Receptor Maturation

(A) Multiple sequence alignment of a part of the third extracellular domain (D3) of IL-11R (amino acid residues 220–319) from different mammalian species. Amino acid residues comprising the tryptophan-arginine zipper are indicated in red, and the WSXWS motive is highlighted in gray.

(B) Structural model of the D3 domain of the human IL-11R. Amino acid residues included in the tryptophan-arginine zipper are indicated, and the critical arginine 296 is highlighted in red.

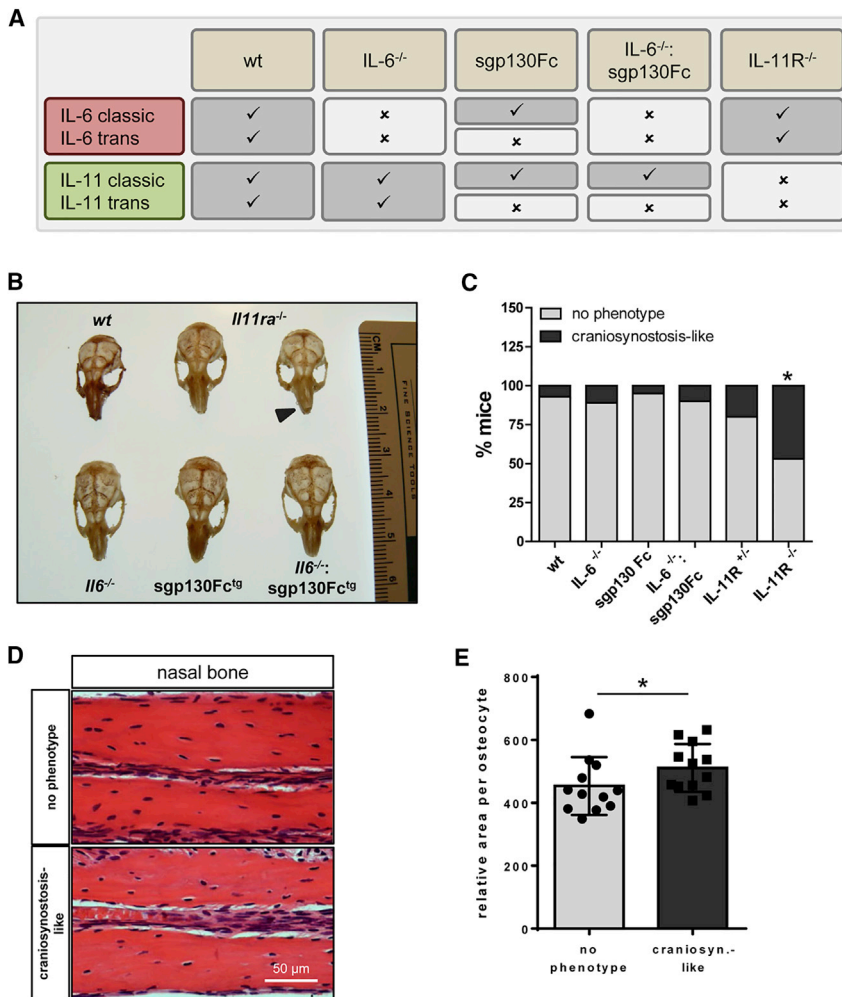(C and D) Point mutations targeting the single arginine residues of the tryptophan-arginine zipper were introduced into an IL-11R expression plasmid, resulting receptor mutants were expressed in HEK293 cells, (C) cell lysates were analyzed via western blot, and (D) receptor cell surface expression was determined using flow cytometry. Untransfected cells served as negative control (untr). Quantification of the mean fluorescent intensity (mean ± SD) normalized to the wild-type expression (100%) from three independent experiments is depicted (ANOVA, $F_{[5, 21]} = 281.1$, $*p < 0.05$).

See also Figure S2.

A Conserved Tryptophan-Arginine Zipper within the D3 Domain of the IL-11R Is Disturbed by the R296W Mutation

Cytokine receptors, including the IL-11R, contain the highly conserved so-called WSXWS motif (Figure 4A), which is thought to be important for ligand binding, folding, and intracellular trafficking (Yoshimura et al., 1992). Although the R296W patient mutation is not located directly within the WSXWS motif, it is part of a conserved so-called tryptophan-arginine zipper, which includes the WSXWS motif (Figures 4A and 4B; Olsen and Kragelund, 2014). On the basis of this knowledge, we hypothesized that mutations of other residues within this zipper should lead to a similar defect in maturation of the IL-11R and replaced each of the other three arginine residues (Arg-257, Arg-261, and Arg-292) with tryptophan residues, which indeed impaired maturation and cell surface appearance (Figures 4C and 4D).

Interestingly, the IL-6 receptor (IL-6R) contains a similar tryptophan-arginine zipper in its D3 domain (Figure S2A). Mutation of Arg-293 has been shown previously to prevent binding of IL-6 to the IL-6R, but the reason for this had not been investigated (Yawata et al., 1993). Accordingly, maturation of IL-6R-R293W was impaired (Figures S2B and S2C), and a 50% reduction on IL-6R cell surface levels was detected (Figures S2D and S2E). In contrast to their WT counterparts, Ba/F3-gp130-IL-6R-R293W cells did not respond to IL-6 (Figures S2F and S2G), indicating that the tryptophan-arginine zipper of the IL-6R is critical for biological function of the IL-6R.

IL-11 Classic Signaling, but Neither IL-11 *trans*-Signaling nor IL-6 Signaling, Is Required for Proper Skull Formation *In Vivo*

Finally, we analyzed the contribution of both cytokines via their classic and *trans*-signaling pathways for skull formation *in vivo*. Nieminen et al. (2011) had previously reported that some of their *Il11ra*^{−/−} mice had twisted snouts and craniosynostosis-like

---

(D) Stably transduced Ba/F3-gp130 cell lines were stimulated with increasing amounts of recombinant IL-11. Cell viability was measured 48 hr later (mean ± SD; RLU, relative light units).

(E) Release of soluble IL-11R variants carrying a premature stop codon at position Q329 into the cell culture supernatant of transfected HEK293 cells was analyzed as described in (B).

(F and G) Supernatants as shown in (E) were used to stimulate Ba/F3-gp130 cells. Where indicated, 500 ng/mL IL-11 was added. Cell viability (F) was measured after 48 hr, and STAT3-phosphorylation (G) was analyzed using western blotting after 15 min of stimulation.

(H) HEK293 cells were transfected with expression plasmids encoding either sIL-11R-WT or sIL-11R-R296W. The cells were lysed, and 30 μg of the lysates were incubated with IL-11, sgp130Fc, or IL-11 and sgp130Fc or were left untreated. Proteins bound to sgp130Fc were collected via binding to protein G-agarose beads and subsequently analyzed using western blot.

(C and F) Mean ± SD is shown.

Figure 5. Only Mice Lacking IL-11 Classic Signaling Show a Craniosynostosis-like Phenotype

(A) Overview of the mouse strains used in this study and of the functionality of IL-6 and IL-11 signaling pathways. Check marks, functional; X's, non-functional.

(B) Mouse skulls of the indicated phenotypes (n = 15–20 per group) were prepared, and their phenotype was classified by two independent and blinded investigators as either "no phenotype" or "craniosynostosis-like." Representative skulls of each genotype are shown. For *Il11ra*$^{-/-}$ mice, two skulls are depicted, one of them showing a strongly twisted snout (arrowhead).

(C) Proportion of mice with different genetic IL-6 and IL-11 signaling limitations classified as "no phenotype" or "craniosynostosis-like" (Fisher's exact test, *p < 0.05 compared with wild-type).

(D) H&E-stained sections of the nasal bone of decalcified and paraffin-embedded skulls from *Il11ra*$^{-/-}$ mice. One representative picture for each classification is shown.

(E) Quantification of the staining analyses as exemplary shown in (D). Numbers of osteocytes per area of three images per slice were counted (n = 4 mice per group) (Mann-Whitney-U test, *p < 0.05). Mean ± SD is shown.

the left and the right nasal bone and results in the twisted snouts predominantly seen in the *Il11ra*$^{-/-}$ animals. Whether this also occurs in human patients is unknown and warrants further investigations. In summary, our data rule out a contribution of IL-6 to the craniosynostosis phenotype in mice and identify IL-11 classic signaling as the only IL-6 or IL-11 signaling pathway that contributes to correct skull formation in mice.

DISCUSSION

Coding mutations within the gene encoding the IL-11R have been described in patients with craniosynostosis-like phenotypes (Clarke et al., 2018; Keupp et al., 2013; Nieminen et al., 2011). They result in rather heterogeneous clinical phenotypes, which include synostosis of one or multiple sutures, conductive hearing loss, midfacial hypoplasia, supernumerary teeth, and/or tooth eruption failure. It is currently unclear how and if this variability can be attributed to the different mutations of the IL-11R.

Here, we confirm for three of the patient mutations that they render the IL-11R biologically inactive. They do not mature properly and are therefore not transported to the cell surface, which explains their lack of biological activity. Although we identified disturbance of a conserved arginine-tryptophan zipper as the underlying cause of the R296W variant, the molecular reason for the impaired maturation of the other variants is less clear. However, proline residues have been shown to be critical for the stability of fibronectin type III domains (Steward et al.,

features. Therefore, we used different genetically modified mouse strains, which enabled us to dissect the contribution of the individual signaling pathways (Figure 5A) (Agthe et al., 2017). In order to assess the skull development in the individual mouse strains, the skulls were removed, cleaned of soft tissue, and classified by two independent and blinded investigators as either "no phenotype" or "craniosynostosis-like" (Figure 5B). Despite craniofacial abnormalities in some animals, WT, *Il6*$^{-/-}$, sgp130Fc^{tg}, and *Il6*$^{-/-}$:sgp130Fc^{tg} mice had overall normally developed skulls, ruling out a role for IL-6 signaling and IL-11 *trans*-signaling for this developmental process (Figure 5C). Interestingly, heterozygous *Il11ra*$^{+/-}$ mice showed craniosynostosis-like features in 20% of the analyzed mice, and nearly 50% of the homozygous *Il11ra*$^{-/-}$ mice showed this phenotype (Figure 5C).

We furthermore made sections of mouse skulls with and without craniosynostosis-like features of *Il11ra*$^{+/-}$ and *Il11ra*$^{-/-}$ mice (Figure 5D). Despite overall normal development in both groups, we noted a significant increase in the relative area per osteocyte in animals with craniosynostosis-like features (Figure 5E). This finding suggests that the reduction in osteocytes impairs the synchronization of bone growth between

2002), which could explain why IL-11R-P200T is retained intracellularly.

IL-6 has partly overlapping functions with IL-11 and is often considered as the more important member of the IL-6 family (Garbers and Scheller, 2013; Putoczki and Ernst, 2010). Here, we could exclude a role for IL-6 signaling in the formation of the skull, because $Il6^{-/-}$ and sgp130Fc^{tg} mice exhibited no significant features of craniosynostosis, and no craniosynostosis patients with mutations in the IL-6 or the IL-6R genes are known.

In mice, IL-11R deficiency compromises bone development and length of the long bones and affects osteoblast and osteoclast function (Sims et al., 2005). It has recently been shown that IL-11R-knockout animals also display skull abnormalities, which partly resemble the phenotype observed in human patients (Nieminen et al., 2011). We could confirm this observation, as nearly 50% of the $Il11ra^{-/-}$ mice analyzed in this study had twisted snouts. Furthermore, using different genetically modified mouse strains, we could show that IL-11 signaling via the membrane-bound IL-11R is required for proper skull development, while IL-11 *trans*-signaling via the soluble IL-11R is dispensable in this context. Interestingly, IL-11 *trans*-signaling has recently been shown to be involved in cardiovascular fibrosis, making the specific inhibition of this pathway a potential therapeutic option, which would possibly not interfere with bone development and metabolism and thus be an important safety aspect of anti-IL-11 therapy (Schafer et al., 2017).

In summary, our study uncovers the molecular reasons for the defects in IL-11 signaling in craniosynostosis patients with mutations in the IL-11R and shows that only the IL-11 classic signaling pathway is required for skull development *in vivo*.

STAR★METHODS

Detailed methods are provided in the online version of this paper and include the following:

- KEY RESOURCES TABLE
- CONTACT FOR REAGENT AND RESOURCE SHARING
- EXPERIMENTAL MODEL AND SUBJECT DETAILS
  - Cultivation of HEK293, HeLa and Phoenix-Eco cell lines
  - Mouse strains
- METHOD DETAILS
  - Construction of expression plasmids
  - Cultivation of Ba/F3-gp130 cells and cell lines derived thereof
  - Transduction of Ba/F3-gp130 cells
  - Ba/F3-gp130 cell proliferation assay and detection of (p)STAT3
  - Transfection of cells, cell lysis and precipitation of supernatants
  - Deglycosylation of cell lysates
  - Western blotting
  - Flow cytometry
  - Immunofluorescence staining and confocal microscopy

- Co-precipitation of IL-11 and sIL-11R via sgp130Fc
- Preparation of murine head bones and staining of slices
- QUANTIFICATION AND STATISTICAL ANALYSIS
  - Quantification
  - Statistical analysis

AUTHOR CONTRIBUTIONS

C.G. conceived the project and designed the experiments. M.A., J.B., M.W., B.K., P.A., C.M.F., J.L., S.A.-S., and C.B. contributed to the experiments and analyzed the data. Y.G. advised on and performed the statistical analysis. G.H.W., S.R.-J., and T.P. contributed reagents. C.G. and M.A. wrote the manuscript. J.B., Y.G., M.W., B.K., P.A., C.M.F., J.L., S.A.-S., C.B., S.R.-J., G.H.W., T.P., and J.G. contributed to the final version of the manuscript.

DECLARATION OF INTERESTS

G.H.W. is an inventor on patents protecting improved sgp130 and sgp130Fc variants and is employed by CONARIS Research Institute, which has outlicensed its interleukin-6 inhibitor olamkicept to Ferring Pharmaceuticals. S.R.-J. has acted as a consultant and speaker to Chugai, Genentech Roche, AbbVie, Sanofi, and Pfizer. He also declares that he is an inventor on patents owned by CONARIS Research Institute, which develops the sgp130Fc protein (olamkicept) together with Ferring Pharmaceuticals, and he has stock ownership in CONARIS. All other authors declare no competing interests.

REFERENCES

Agthe, M., Garbers, Y., Putoczki, T., and Garbers, C. (2017). Interleukin-11 classic but not trans-signaling is essential for fertility in mice. Placenta *57*, 13–16.

Agthe, M., Garbers, Y., Grötzinger, J., and Garbers, C. (2018). Two N-linked glycans differentially control maturation, trafficking and proteolysis, but not activity of the IL-11 receptor. Cell. Physiol. Biochem. *45*, 2071–2085.

Baumann, H., and Schendel, P. (1991). Interleukin-11 regulates the hepatic expression of the same plasma protein genes as interleukin-6. J. Biol. Chem. *266*, 20424–20427.

Clarke, C.M., Fok, V.T., Gustafson, J.A., Smyth, M.D., Timms, A.E., Frazar, C.D., Smith, J.D., Birgfeld, C.B., Lee, A., Ellenbogen, R.G., et al. (2018). Single suture craniosynostosis: Identification of rare variants in genes associated with syndromic forms. Am. J. Med. Genet. A. *176*, 290–300.

Davidson, A.J., Freeman, S.A., Crosier, K.E., Wood, C.R., and Crosier, P.S. (1997). Expression of murine interleukin 11 and its receptor alpha-chain in adult and embryonic tissues. Stem Cells *15*, 119–124.

Garbers, C., and Scheller, J. (2013). Interleukin-6 and interleukin-11: same same but different. Biol. Chem. *394*, 1145–1161.

Garbers, C., Hermanns, H.M., Schaper, F., Müller-Newen, G., Grötzinger, J., Rose-John, S., and Scheller, J. (2012). Plasticity and cross-talk of interleukin 6-type cytokines. Cytokine Growth Factor Rev. *23*, 85–97.

Keupp, K., Li, Y., Vargel, I., Hoischen, A., Richardson, R., Neveling, K., Alanay, Y., Uz, E., Elcioğlu, N., Rachwalski, M., et al. (2013). Mutations in the interleukin receptor IL11RA cause autosomal recessive Crouzon-like craniosynostosis. Mol. Genet. Genomic Med. *1*, 223–237.

Lokau, J., Agthe, M., and Garbers, C. (2016a). Generation of soluble inter-leukin-11 and interleukin-6 receptors: a crucial function for proteases during inflammation. Mediators Inflamm. *2016*, 1785021.

Lokau, J., Nitz, R., Agthe, M., Monhasery, N., Aparicio-Siegmund, S., Schu-macher, N., Wolf, J., Möller-Hackbarth, K., Waetzig, G.H., Grötzinger, J., et al. (2016b). Proteolytic cleavage governs interleukin-11 trans-signaling. Cell Rep. *14*, 1761–1773.

Lokau, J., Agthe, M., Flynn, C.M., and Garbers, C. (2017). Proteolytic control of Interleukin-11 and Interleukin-6 biology. Biochim. Biophys. Acta *1864* (*11 Pt B*), 2105–2117.

Lokau, J., Göttert, S., Arnold, P., Düsterhöft, S., Massa López, D., Grötzinger, J., and Garbers, C. (2018). The SNP rs4252548 (R112H) which is associated with reduced human height compromises the stability of IL-11. Biochim. Bio-phys. Acta *1865*, 496–506.

Monhasery, N., Moll, J., Cuman, C., Franke, M., Lamertz, L., Nitz, R., Görg, B., Häussinger, D., Lokau, J., Floss, D.M., et al. (2016). Transcytosis of IL-11 and apical redirection of gp130 is mediated by IL-11α receptor. Cell Rep. *16*, 1067–1081.

Morriss-Kay, G.M., and Wilkie, A.O.M. (2005). Growth of the normal skull vault and its alteration in craniosynostosis: insights from human genetics and exper-imental studies. J. Anat. *207*, 637–653.

Nieminen, P., Morgan, N.V., Fenwick, A.L., Parmanen, S., Veistinen, L., Mik-kola, M.L., van der Spek, P.J., Giraud, A., Judd, L., Arte, S., et al. (2011). Inac-tivation of IL11 signaling causes craniosynostosis, delayed tooth eruption, and supernumerary teeth. Am. J. Hum. Genet. *89*, 67–81.

Nitz, R., Lokau, J., Aparicio-Siegmund, S., Scheller, J., and Garbers, C. (2015). Modular organization of Interleukin-6 and Interleukin-11 α-receptors. Bio-chimie. *119*, 175–182.

Olsen, J.G., and Kragelund, B.B. (2014). Who climbs the tryptophan ladder? On the structure and function of the WSXWS motif in cytokine receptors and thrombospondin repeats. Cytokine Growth Factor Rev. *25*, 337–341.

Putoczki, T., and Ernst, M. (2010). More than a sidekick: the IL-6 family cyto-kine IL-11 links inflammation to cancer. J. Leukoc. Biol. *88*, 1109–1117.

Putoczki, T.L., Thiem, S., Loving, A., Busuttil, R.A., Wilson, N.J., Ziegler, P.K., Nguyen, P.M., Preaudet, A., Farid, R., Edwards, K.M., et al. (2013). Interleukin-11 is the dominant IL-6 family cytokine during gastrointestinal tumorigenesis and can be targeted therapeutically. Cancer Cell *24*, 257–271.

Rice, D.P.C. (2005). Craniofacial anomalies: from development to molecular pathogenesis. Curr. Mol. Med. *5*, 699–722.

Schafer, S., Viswanathan, S., Widjaja, A.A., Lim, W.W., Moreno-Moral, A., DeLaughter, D.M., Ng, B., Patone, G., Chow, K., Khin, E., et al. (2017). IL-11 is a crucial determinant of cardiovascular fibrosis. Nature *552*, 110–115.

Sims, N.A., Jenkins, B.J., Nakamura, A., Quinn, J.M., Li, R., Gillespie, M.T., Ernst, M., Robb, L., and Martin, T.J. (2005). Interleukin-11 receptor signaling is required for normal bone remodeling. J. Bone Miner. Res. *20*, 1093–1102.

Steward, A., Adhya, S., and Clarke, J. (2002). Sequence conservation in Ig-like domains: the role of highly conserved proline residues in the fibronectin type III superfamily. J. Mol. Biol. *318*, 935–940.

Yawata, H., Yasukawa, K., Natsuka, S., Murakami, M., Yamasaki, K., Hibi, M., Taga, T., and Kishimoto, T. (1993). Structure-function analysis of human IL-6 receptor: dissociation of amino acid residues required for IL-6-binding and for IL-6 signal transduction through gp130. EMBO J. *12*, 1705–1712.

Yoshimura, A., Zimmers, T., Neumann, D., Longmore, G., Yoshimura, Y., and Lodish, H.F. (1992). Mutations in the Trp-Ser-X-Trp-Ser motif of the erythropoi-etin receptor abolish processing, ligand binding, and activation of the receptor. J. Biol. Chem. *267*, 11619–11625.

STAR★METHODS

KEY RESOURCES TABLE

REAGENT or RESOURCE	SOURCE	IDENTIFIER
Antibodies		
anti-pSTAT3 (Y705)	Cell Signaling	Clone D3A7, Cat#9145
anti-STAT3	Cell Signaling	Clone 124H6, Cat#9139
anti-myc	Cell Signaling	Clone 71D10, Cat#2278
Anti-GAPDH	Cell Signaling	Clone 14C10, Cat#2118
Anti-IL-11	R&D Systems	Cat#DY218
Anti-Actinin	Cell Signaling	CloneD6F6, Cat#6487
Anti-IL-6R	Lokau et al., 2016b	4-11
Anti-GM130	BD Bioscience	Clone 35/GM130, Cat#610822
AlexaFlour488 anti-rabbit	Thermo Fisher Scientific	Cat#A-11034
AlexaFlour488 anti-mouse	Thermo Fisher Scientific	Cat#A-11001
Anti-rabbit-POD	Dianova	Cat#111-035-003
Anti-mouse-POD	Dianova	Cat#115-035-003
Anti-human-POD	Dianova	Cat#109-035-088
Bacterial and Virus Strains		
XL1-Blue	Stratagene	N/A
Chemicals, Peptides, and Recombinant Proteins		
Hyper-IL-6	Nitz et al., 2015	N/A
IL-6	Nitz et al., 2015	N/A
IL-11	Nitz et al., 2015	N/A
BoxI	ThermoFisher Scientific	Cat#ER1431
KfII	ThermoFisher Scientific	Cat#FD2164
PmII	ThermoFisher Scientific	Cat#ER0361
Eco81I	ThermoFisher Scientific	Cat#ER0371
NotI	ThermoFisher Scientific	Cat#ER0591
TurboFect	ThermoFisher Scientific	Cat#R0531
Polybrene	Sigma Aldrich	Cat# H9268
Puromycin	Carl Roth	Cat#0240.1
trichloracetic acid	Carl Roth	Cat#8789.2
Acetone	Carl Roth	Cat#9780.1
Tris-HCl	Carl Roth	Cat#A411.1
NaCl	Carl Roth	Cat#P029.1
Triton X-100	Carl Roth	Cat#1052.1
cOmplete protease inhibitor cocktail	Roche Applied Science	Cat#000000011697498001
PNGaseF	New England Biolabs	Cat#P0705S
EndoH	New England Biolabs	Cat#P0702S
Tween 20	Carl Roth	Cat#9127.1
SDS	Carl Roth	Cat#0183.1
β-mercaptoethanol	Carl Roth	Cat#4227.3
bovine serum albumin	Carl Roth	Cat#9638.1
Paraformaldehyde	Carl Roth	Cat#0335.1
Glycine	Carl Roth	Cat#3187.1
EDTA	Carl Roth	Cat#3053.1
Critical Commercial Assays		
CellTiter Blue Viability Assay	Promega	Cat#G8080

(Continued on next page)

Continued

REAGENT or RESOURCE	SOURCE	IDENTIFIER
Experimental Models: Cell Lines		
HEK293	ATCC	RRID:CVCL_0045
Ba/F3	DSMZ	RRID:CVCL_0161
HeLa	ATCC	RRID:CVCL_0030
Experimental Models: Organisms/Strains		
$Il6^{-/-}$: B6.129S2-$Il6^{tm1Kopf}$/J	The Jackson Laboratory	RRID:MGI:3629043
$Il11ra^{-/-}$: B6.129S1-$Il11ra1^{tm1Wehi}$/J	The Jackson Laboratory	RRID:MGI:3604405
sgp130Fc^{tg}	Agthe et al., 2017	N/A
$Il6^{-/-}$:sgp130Fc^{tg}	Agthe et al., 2017	N/A
Recombinant DNA		
pcDNA3.1-myc-hIL-11R	Nitz et al., 2015	N/A
pcDNA3.1-myc-hIL-11-R296W	This study	N/A
pcDNA3.1-myc-hIL-11-P200T	This study	N/A
pcDNA3.1-myc-hIL-11-P221R	This study	N/A
pcDNA3.1-myc-hIL-11-KKSS	This study	N/A
pcDNA3.1-myc-hIL-11-R296K	This study	N/A
pcDNA3.1-myc-hIL-11-R296H	This study	N/A
pcDNA3.1-myc-hIL-11-R296A	This study	N/A
pcDNA3.1-myc-hIL-11-R296V	This study	N/A
pcDNA3.1-myc-hIL-11-R296F	This study	N/A
pcDNA3.1-myc-hIL-11-R296M	This study	N/A
pcDNA3.1-myc-hIL-11-R296L	This study	N/A
pcDNA3.1-myc-hIL-11-R296I	This study	N/A
pcDNA3.1-myc-hIL-11-R296P	This study	N/A
pcDNA3.1-myc-hIL-11-R296Q	This study	N/A
pcDNA3.1-myc-hIL-11-R296G	This study	N/A
pcDNA3.1-myc-hIL-11-R296T	This study	N/A
pcDNA3.1-myc-hIL-11-R296S	This study	N/A
pcDNA3.1-myc-hIL-11-R296C	This study	N/A
pcDNA3.1-myc-hIL-11-R296N	This study	N/A
pcDNA3.1-myc-hIL-11-R296Y	This study	N/A
pcDNA3.1-myc-hIL-11-R296E	This study	N/A
pcDNA3.1-myc-hIL-11-R296D	This study	N/A
pcDNA3.1-myc-hsIL-11-R296W	This study	N/A
pcDNA3.1-myc-hsIL-11-R296A	This study	N/A
pcDNA3.1-myc-hsIL-11-R296K	This study	N/A
pcDNA3.1-myc-hIL-11-R257W	This study	N/A
pcDNA3.1-myc-hIL-11-R261W	This study	N/A
pcDNA3.1-myc-hIL-11-R292W	This study	N/A
pcDNA3.1-hIL-6R	Nitz et al., 2015	N/A
pcDNA3.1-hIL-6R-R293W	This study	N/A
pMOWS-myc-hIL-11R	Nitz et al., 2015	N/A
pMOWS-myc-hIL-11-R296W	This study	N/A
pMOWS-myc-hIL-11-P200T	This study	N/A
pMOWS-myc-hIL-11-P221R	This study	N/A
pMOWS-myc-hIL-11-R296A	This study	N/A

CONTACT FOR REAGENT AND RESOURCE SHARING

Further information and requests for resources and reagents should be directed to and will be fulfilled by the Lead Contact, Christoph Garbers (christoph.garbers@med.ovgu.de).

EXPERIMENTAL MODEL AND SUBJECT DETAILS

Cultivation of HEK293, HeLa and Phoenix-Eco cell lines

All cell lines were cultured in DMEM medium [10% fetal bovine serum (FBS), penicillin (60 mg/l) and streptomycin (100 mg/l)]. They were maintained in a standard incubator at 37°C with 5% CO_2 in a water-saturated atmosphere. Cells were routinely passaged twice a week at a 1:10 ratio. The sex of the cell lines is female. Cell lines were obtained from official repositories, and therefore no additional cell authentication was performed.

Mouse strains

18 weeks old mice of the following strains were used in this study: $Il11ra^{-/-}$, $Il6^{-/-}$, sgp130Fc^{tg} and $Il6^{-/-}$:sgp130Fc^{tg} and corresponding control animals. All strains are on the same genetic background (C57BL/6) and were backcrossed for at least 10 generations before the experiments were performed. 15–20 animals per group (equal proportions of male/female) were used. There is no indication in the literature that the observed craniosynostosis-like features are influenced by the sex of the mice. Furthermore, we observed no correlation between sex and craniosynostosis-like features in our study and therefore included male and female animals. All experiments were performed in accordance with the local guidelines for animal care and protection (Büro des Tierschutzbeauftragten der CAU zu Kiel, study #963).

METHOD DETAILS

Construction of expression plasmids

The expression plasmid encoding the human IL-11R tagged with N-terminal c-*myc* (pcDNA3.1-myc-hIL-11R) and the IL-6R (pcDNA3.1-hIL-6R) were described previously (Nitz et al., 2015). All other receptor mutants containing a single amino acid substitution were constructed via standard splicing by overlap extension PCR and inserted into the respective WT vector by using BstEII/NotI (IL-11R) or Eco81I/NotI (IL-6R) restriction sites. Expression plasmids encoding soluble IL-11R variants were created by insertion of a premature stop codon just before the transmembrane domain (Q329X). For stable transduction of Ba/F3-gp130 cells, the open reading frames were subcloned into pMOWS plasmids by using BoxI/KflI (IL-11R) or KflI/PmlI (IL-6R) restriction sites.

Cultivation of Ba/F3-gp130 cells and cell lines derived thereof

Ba/F3-gp130 cells and cell lines derived thereof were cultured in DMEM medium [10% fetal bovine serum (FBS), penicillin (60 mg/l) and streptomycin (100 mg/l)]. They were maintained in a standard incubator at 37°C with 5% CO_2 in a water-saturated atmosphere. The culture medium for Ba/F3-gp130 cells additionally contained 10 ng/ml Hyper-IL-6. After stable transduction, Ba/F3-gp130-IL-11R cells and all other cell lines that expressed a biologically active IL-11R were cultured with 10 ng/ml recombinant IL-11 instead. Likewise, Ba/F3-gp130-IL-6R cells and all other cell lines that expressed a biologically active IL-6R were instead cultured with 10 ng/ml recombinant IL-6. The sex of Ba/F3 cells is unknown. The cell line was obtained from an official repositories, and therefore no additional cell authentication was performed.

Transduction of Ba/F3-gp130 cells

A retroviral system was used to stably transduce BaF3-gp130 cells. To this end, the generated 2μg pMOWS plasmids were transiently transfected in 8×10^5 Phoenix-Eco cells using Turbofect according to the manufacturer's instructions. Retroviral supernatants were filtered through a sterile filter in order to remove debris of the Phoenix-Eco cells. 250 μl of the retroviral supernatants were mixed with 8μg/ml Polybrene solution and centrifuged with 1×10^5 Ba/F3-gp130 cells at 800 x g for 2 h at room temperature.

Afterward, the cells were grown in standard medium supplemented with 10 ng/ml Hyper-IL-6. 48 hours later, cells were selected with 1.5 μg/ml puromycin for two weeks. Cells were then cultivated with either 10 ng/ml IL-6 or IL-11 where appropriate.

Ba/F3-gp130 cell proliferation assay and detection of (p)STAT3

The response of different Ba/F3-gp130 cell lines to IL-11 or IL-6 was measured via the CellTiter Blue Viability Assay (Promega, Karls-ruhe, Germany) according to the manufacturer's instructions in a 96 well plate. 5,000 cells per well were stimulated with increasing amounts of IL-11 or IL-6 (0 – 100 ng/ml) for 48 h at 37°C. After adding the reaction reagent the fluorescence intensity was measured and normalized to the value obtained at the starting point. Additionally, pSTAT3 levels in the different Ba/F3-gp130 cell lines were determined as follows. Cells were washed twice in PBS, serum-starved for 2.5 h and stimulated with recombinant cytokine (10 ng/ml) for 15 min. Afterward, cells were collected via centrifugation, boiled in 2.5x Laemmli buffer, separated on 10% SDS gels and analyzed via semi-dry western blotting.

Transfection of cells, cell lysis and precipitation of supernatants

HEK293 cells were seeded on 10 cm culture dishes and transfected the following day with 5 μg DNA using Turbofect (Thermo Scientific, Bonn, Germany). 48 h after transfection cells were either directly harvested or incubated with serum-free medium in order to analyze constitutive receptor release (4 or 6 h at 37°C). Supernatants were harvested and then subjected to trichloracetic acid (TCA)-precipitation. Here, 1 mL supernatant was subjected to a two-step centrifugation protocol (first at 1,200 × g and then at 18,000 × g). Supernatants were afterward mixed with 20% TCA at a 1:1 ration and incubated on ice for 20 min. Precipitates were collected by centrifugation at 18,000 × g. After discarding of the supernatants, the precipitated proteins were washed with 350 μL ice-cold acetone and centrifuged again (18,000 × g). Pellets were dried at room temperature after the acetone was removed by pipetting. Finally, the pellets were boiled in Laemmli buffer subjected to semi-dry western blot analysis. Cells were lysed in lysis buffer [50 mM Tris-HCl pH 7.5, 150 mM NaCl, 1% Triton X-100 and cOmplete protease inhibitor cocktail (Roche Applied Science, Penzberg, Germany) according to the manufacturer's instructions]. Supernatant and cell lysates were analyzed by semi-dry western blotting.

Deglycosylation of cell lysates

15 μg protein from cell lysates were denatured at 95°C for 10 min and then incubated with 500 units of PNGaseF or EndoH overnight at 37°C. Deglycosylated samples were boiled in 5x Laemmli buffer (10 min at 95°C) and subjected to western blot analysis.

Western blotting

Protein lysates and TCA-precipitated proteins were separated by SDS-PAGE under reducing conditions. Proteins were afterward transferred to a PVDF membrane (GE Healthcare), which were then blocked with a solution of 5% skim milk powder dissolved in TBS-T (10 mm Tris-HCl, pH 7.6, 150 mm NaCl, and 0.05% Tween 20). The membrane was probed with the indicated primary antibodies at 4°C overnight. Membranes were washed afterward with TBS-T at least three times and probed with an appropriate secondary antibody conjugated to horseradish peroxidase. Proteins were detected with ECL Prime western blotting detection reagent (GE Healthcare) according to the manufacturer's instructions. To detect proteins serving as loading controls, membranes were cut with a scalpel when different molecular weights of the proteins of interest allowed this, and the protein serving as loading control was detected as described above. For proteins having similar molecular weights (e.g., pSTAT3/STAT3), membranes were stripped after detection of the phosphorylated protein with stripping buffer (62.5 mm Tris-HCl, pH 6.8, 2% SDS, 0.1% β-mercaptoe-thanol, for 30 min at 60°C), washed 3 times with TBS-T, blocked again with a solution of 5% skim milk powder dissolved in TBS-T, and incubated with the antibody directed against the non-phosphorylated protein.

Flow cytometry

Transfected HEK293 cells or stably transduced Ba/F3-gp130 cell lines were used. Cells were washed once in 1% bovine serum albumin/phosphate-buffered saline (BSA/PBS), extracellularly stained against IL-11R or IL-6R for 60 min at 4°C (anti-myc-tag or 4-11 antibody, respectively; 1:100 in 1% BSA/PBS) and washed three times in 1% BSA/PBS. Subsequently, cells were incubated with a secondary AlexaFlour488 anti-rabbit or anti-mouse antibody (1:100 in 1% BSA/PBS) for 60 min at 4°C and washed three times. Receptor surface expression was analyzed on a BD FACS CantoII (BD Biosciences) using the FACS Diva software and FCS Express (*De Novo* Software, Los Angeles, California, US).

Immunofluorescence staining and confocal microscopy

HeLa cells were seeded on coverslips and transfected as described above for HEK293 cells. 48 h after transfection cells were fixed with 4% paraformaldehyde/PBS at room temperature for 10 min, incubated in 0.12% Glycine/PBS for 10 min at RT and blocked with 10% FBS/PBS for 60 min at RT. Coverslips were stained with anti-myc-tag mAb (1:200 in blocking solution) at RT for 60 min, washed five times with PBS and stained with a secondary AlexaFluor488-conjugated antibody (1:300 in blocking solution) again for 60 min at RT. After further washing (five times in PBS and two times in ddH2O), cells were mounted with ProLong Gold Antifade reagent containing DAPI (Invitrogen/Life Technologies, Darmstadt, Germany). For intracellular stainings the same protocol as described above was used, but 0.2% saponin was added to the blocking solution. For co-staining with the Golgi marker GM130, the intracellular

staining protocol was applied and both primary antibodies (anti-myc and anti-GM130; diluted 1:200 in blocking solution) as well as both secondary antibodies (anti-rabbit AlexaFluor488 and anti-mouse AlexaFluor594; diluted 1:300 in blocking solution) were co-incubated. Stainings were examined on a confocal laser scanning microscope (Olympus FluoView FV1000) with a 60x oil-immersion objective (NA:1.35) at RT. Co-localization of IL-11R and GM130 was analyzed via the ImageJ plugin JACoP (NIH, Bethesda, MD, US) and expressed by the Manders' M2 overlap coefficient.

Co-precipitation of IL-11 and sIL-11R via sgp130Fc

500 ng recombinant IL-11, 10 μg sgp130Fc and 30 μg lysate of transfected HEK293 cells expressing either sIL-11R-wt or sIL-11R-R296W were incubated in PBS for 1 h at 37°C. Afterward, protein G-agarose beads (Merck, Darmstadt, Germany) were used to pre-cipitate protein complexes overnight at 4°C. Subsequently beads were washed in PBS, boiled in 5x Laemmli buffer and analyzed by western blotting.

Preparation of murine head bones and staining of slices

For analysis of murine head bone phenotypes, skulls of mice on a C57BL/6 background older than 18 weeks were removed and cleaned from soft tissue. Skulls were fixed in 4% PFA and classified according to their phenotype (''no phenotype'' or ''cranio-synostosis-like'') by two independent and blinded investigators. Additionally, skulls were decalcified for 6 weeks in 1% EDTA supplemented with 1% PFA. After embedding of the skulls into paraffin, 7-μm sections were prepared, stained in hematoxylin/eosin according to standard histological procedures, and the nasal bone was examined. A total of 3 individual images were taken per animal, and the number of osteocytes was determined per bone area. For this purpose, individual areas were selected, and the num-ber of osteocytes was counted using the software ImageJ.

QUANTIFICATION AND STATISTICAL ANALYSIS

Quantification

Mouse osteocytes were counted using the software ImageJ. Co-localization of IL-11R and GM130 was analyzed via the ImageJ plu-gin JACoP (NIH, Bethesda, MD, US). Densitometric analysis of western blots was performed using Image Studio Lite 5.2 (LI-COR Biosciences).

Statistical analysis

Mean values (n = 3) and standard deviations are provided in Figures 1B, 1C, 1D, 1E, 2C, 2F, 3C, 3D, 3F, 4D, 5E, S1B, S1C, S1D, S2B, S2C, S2E, S2F and S2G. Comparison of two groups was done in GraphPad Prism (GraphPad, La Jolla, CA) by the Mann-Whitney-U test (Figures 3F and 5E). For comparisons of multiple groups, one-way analysis of variance (ANOVA) was used and Dun-nett's Multiple Comparison Test was applied (Figures 2C, 2F, 4D, S1C, S1D and S2E). Fisher's exact test was used for the analysis of craniosynostosis in the different mouse strains (Figure 5C). A p value < 0.05 was considered as statistically significant. All information are additionally given in the respective figure legends.